PAPERS IN PHYSICS, VOL. 18, ART. 180002 (2026)

www.papersinphysics.org

Received: 11 January 2025, Accepted: 25 November 2025
Edited by: Francisco Melo, Universidad de Santiago de Chile, Chile

DOI: https://doi.org/10.4279/PIP.180002

ISSN 1852-4249

Green synthesis, characterization, and antibacterial efficiency of copper oxide nanoparticles using *Mitragyna speciosa* (Korth.) Havil leaf extract

Voranuch Thongpool[1]*, Sarawut Jaiyen[1], Akapong Phunpueok[1], Nuchita Sukprasit[1], Atipong Bootchanont[1]

Copper oxide nanoparticles (CuO NPs) possess versatile properties that make them valuable in various applications, including electronics, catalysis, sensing, and biomedical fields. However, conventional synthesis routes often require high energy input, hazardous chemicals, and generate environmentally problematic byproducts. In this work, CuO NPs were synthesized through an eco-friendly green method using *Mitragyna speciosa* (Korth.) Havil leaf extract, whose phytochemicals function as natural reducing and stabilizing agents. The nanoparticles were characterized using UV–visible spectroscopy, FESEM–EDS, and XRD. The optical spectrum exhibited an absorption maximum at ∼480 nm, and the corrected Tauc analysis yielded an indirect band gap of 1.57 eV. XRD analysis confirmed the formation of monoclinic CuO with crystallite sizes of 82–98 nm (Scherrer and Williamson–Hall methods), consistent with FESEM particle sizes of 50–80 nm. Antibacterial tests revealed activity against both *Escherichia coli* and *Staphylococcus aureus*, with minimum inhibitory concentrations (MICs) of 3.98×10^4 μg/mL and 1.00×10^5 μg/mL, respectively. These results demonstrate that *M. speciosa*-mediated synthesis offers a viable, cost-effective, and sustainable approach for producing functional CuO nanoparticles, thereby supporting their potential in future environmental and biomedical applications.

I Introduction

Nanotechnology encompasses the manipulation and engineering of matter at dimensions typically below 100 nm, where physicochemical behaviors differ markedly from those of bulk materials. At this scale, size-dependent phenomena such as quantum confinement, enhanced surface reactivity, and altered electronic structures become dominant, giving rise to new opportunities in electronics, catalysis, sensing, energy storage, and biomedical systems [1, 2]. Metal oxide nanoparticles possess distinctive optical, electronic, and magnetic properties, drawing significant attention and extensive research. Due to these outstanding properties, their use has been applied in several industries, such as: electronics, cosmetic, agriculture, food, and medicine [3, 4].

Copper oxide nanoparticles (CuO NPs) are transition metal oxides that have attracted attention among researchers due to their electrical, magnetic, optical, and physical properties. CuO is a p-type semiconductor with a narrow bandgap (between 1.2 eV and 1.7 eV) [5–10]. It is also useful for solar energy conversion, photothermal applications, catalysis, field emission, gas sensors, and photoconductive devices. CuO NPs can be synthesized by various methods, such as hydrothermal [11], sonochemical [12], thermal oxidation [13], thermal decomposition [14], and precipitation [15], etc. Despite their effectiveness, many of these techniques require elevated temperatures, long reaction times, and/or toxic chemicals, and may generate hazardous byprod-

* voranut_t@rmutt.ac.th

[1] Division of Physics, Faculty of Science and Technology, Rajamangala University of Technology Thanyaburi, Pathum Thani 12110, Thailand.

ucts. Therefore, there is increasing interest in developing environmentally benign synthetic strategies.

Plant-mediated green synthesis has emerged as a promising alternative for fabricating CuO NPs. In such approaches, phytochemicals derived from plant tissues function as reducing, complexing, and capping agents, enabling the formation of stable nanoparticles under mild conditions. Green synthesis offers several advantages: it is simple, non-toxic, low-cost, and compatible with large-scale preparation, while the resulting nanoparticles often show good stability due to surface functionalization by plant-derived molecules [16–22].

Green synthesis has become a crucial aspect of producing CuO NPs. According to the literature review, it was found that various plants have previously been used to synthesize CuO NPs, including *Moringa Oleifera* [23], *Gloriosa superba L.* [5], *Eucalyptus globoulus* [7], *Couroupita guianensis* [24], *Ephedra alata* [25], and *Solanum macrocarpon* fruit [26], etc.

Mitragyna speciosa (Korth.) Havil is a tree native to Thailand and Malaysia that thrives in moist environments and partial sunlight. In Thailand, it is predominantly found in the southern region but can also be cultivated successfully in the central region, including Pathum Thani province. Previous studies have reported that *Mitragyna speciosa* (Korth.) Havil exhibits a range of biological activities, such as anti-inflammatory, antinociceptive, antioxidant, and antibacterial effects. Its leaf extract contains various phytochemicals, including tannins, alkaloids, flavonoids, polyphenols, saponins, and steroids [27–29]. These constituents provide multiple functional groups (e.g., hydroxyl, carbonyl, and amine) capable of interacting with metal ions and stabilizing nanoparticles.

X-ray diffraction (XRD) analysis provides essential insights into crystallinity and microstructural parameters of nanomaterials. The commonly applied Debye–Scherrer equation estimates crystallite size from peak broadening; however, this approach attributes the broadening solely to size effects and does not account for other contributions such as lattice strain, structural imperfections, or defect-induced distortions. To obtain a more complete description of peak broadening, methods such as the Warren–Averbach approach, Rietveld refinement, and the Williamson–Hall (W–H) model have been developed. The W-H model incorporates crystal imperfections and assumes conditions like uniform stress, anisotropic strain, and consistent energy density, enabling the determination of strain, stress, and energy density through its plot [30–32].

In this study, CuO nanoparticles were synthesized using *Mitragyna speciosa* (Korth.) Havil leaf extract as a dual-function reducing and stabilizing agent. The morphology, elemental composition, and optical properties of the CuO NPs were investigated using field emission scanning electron microscopy (FESEM), energy-dispersive X-ray spectroscopy (EDS), and UV–visible spectroscopy, respectively. Detailed XRD peak profile analysis, employing both the Debye–Scherrer and Williamson–Hall methods, was conducted to determine the crystallite size and lattice strain. Furthermore, the antibacterial activity of the synthesized CuO NPs against *Escherichia coli* and *Staphylococcus aureus* was evaluated using the broth dilution method.

II Experimental

i Materials

The copper (II) nitrate trihydrate, $Cu(NO_3)_2$ (with a purity of 99.5%), was obtained from Loba Chemie. The Sodium hydroxide (NaOH) pellets were acquired from QRëC. All the remaining chemicals have been utilized without further modification. The experiments have utilized deionized (D.I.) water.

ii Preparation of *Mitragyna speciosa* (Korth.) Havil leaf powder

The *Mitragyna speciosa* (Korth.) Havil leaves used in this study were grown in Pathum Thani Province, Thailand. The collected *Mitragyna speciosa* (Korth.) Havil leaves were carefully selected to ensure they were free from bruises and insects. The collected *Mitragyna speciosa* (Korth.) Havil leaves were soaked in tap water to remove contaminants and then dehydrated at room temperature. After that, the *Mitragyna speciosa* (Korth.) Havil leaves were torn into small pieces and subjected to dry in a hot air oven at 50 °C for 72 h before being finely powdered using a mortar in the laboratory.

iii Preparation of the *Mitragyna speciosa* (Korth.) Havil leaf extract

Preparation of the *Mitragyna speciosa* (Korth.) Havil leaf extract started with 25 grams of *Mitragyna speciosa* (Korth.) Havil leaf powder dissolved in 100 ml of D.I. water and stirred constantly using a magnetic stirrer at 60 °C for 30 min. The extracted *Mitragyna speciosa* (Korth.) Havil leaf was cooled to room temperature and

subsequently filtered through Whatman No. 1 filter paper. The resultant filtrate can be used immediately or stored at 4 °C for later use.

iv Synthesis of CuO NPs

The general method for synthesizing CuO NPs involves dissolving 1.0 M of $Cu(NO_3)_2$ in 100 ml of D.I. water. Subsequently, 50 mL of *Mitragyna speciosa* (Korth.) Havil leaf extract was introduced to the solution and stirred for 1 h. Subsequently, the pH was adjusted to 8 by adding a 1 M NaOH solution. The formation of CuO NPs could be seen as a shift from blue to green in the admixture. The admixture was left at an ambient temperature for 24 h. Following this duration, a visible, dark brown residue could be observed without the use of any optical device. The residues were acquired using centrifugation at 6000 rpm for 15 min. Subsequently, they were dried in a hot air oven at 105 °C for 24 h. The dark brown residue was calcinated at 400 °C for 2 h in a muffle furnace.

v Characterization

The optical properties of the synthesized CuO NPs were examined using a UV-visible spectrophotometer (UV-vis, PG Instruments - Model T60) within the wavelength spectrum of 200–1100 nm. The morphology and element composition of synthesized CuO NPs were analyzed using a JEOL-JSM7800F field emission scanning electron microscope (FESEM) and Oxford X-Max 20 energy dispersive X-ray spectroscopy (EDS) combined with FESEM. Additionally, the microstructural properties of the synthesized CuO NPs were determined using an X-ray powder diffractometer equipped with Cu-Kα radiation (XRD, Bruker AXS - Model D8 Advance). XRD patterns were recorded with a 0.02° step size over a 2θ range of 30–90°. The analysis revealed details about the sample's phase, purity, crystallite size, and lattice strain, with crystallite size and strain determined using the Scherrer equation and Williamson-Hall plot.

vi The antibacterial efficacy of the synthesized CuO NPs

The antibacterial efficacy of the synthesized CuO NPs was evaluated using the conventional broth dilution method (CLSI M07-A8), which included monitoring the visible growth of microbes in agar broth. The minimum inhibitory concentration (MIC) of the synthesized CuO NPs in BHI broth was determined by a range of dilutions from 0 mg/mL to 100 mg/mL. The bacterial concentration was changed to 4×10^6 CFU/ml, corresponding to 0.5 McFarland's standard. The control sample was incubated in an inoculation broth for 18 h at 37 °C. The MIC endpoint refers to the minimum inhibitory concentration of the synthesized CuO NPs at which no visible growth is observed in the tubes. The MIC values were established by measuring the optical turbidity of the tubes both before and after incubation.

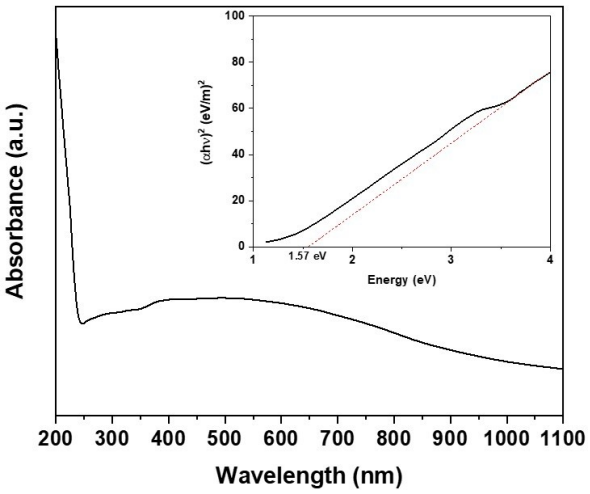

Figure 1: UV-vis spectrum and Tauc plot of synthesized CuO NPs

III Results and discussion

The UV-vis spectrum of the synthesized CuO NPs, shown in Fig. 1, displays a maximum absorption peak at approximately 480 nm, indicating successful synthesis and surface plasmon resonance. The optical band gap (E_g) was calculated by extrapolating the linear region of the $(\alpha h)^2$ vs h plot to the point where $(\alpha h)^2 = 0$, yielding an E_g value of 1.57 eV. This value falls within the typical band-gap range reported for nanostructured CuO (1.2–1.7 eV).

The FESEM image (Fig. 2a) reveals an average particle size below 100 nm, confirming the successful synthesis of CuO NPs. The elemental composition was analyzed via EDS, with the spectrum and percentage composition presented in Fig. 2b. The EDS results detected only copper (Cu) and oxygen (O), with no impu-

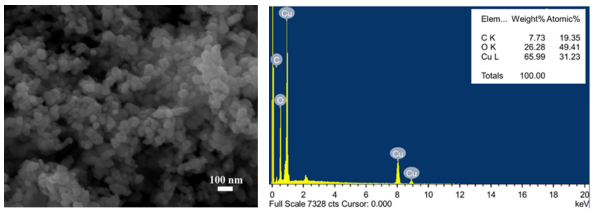

Figure 2: (a) FESEM image and (b) EDS spectrum of synthesized CuO NPs

rities, verifying the purity and successful synthesis of CuO NPs using *Mitragyna speciosa* (Korth). Havil leaf extract.

Phytochemicals present in *M. speciosa* leaf extract include flavonoids, polyphenols, tannins, and alkaloids. These phytochemicals play a crucial role during CuO nanoparticle formation as natural reducing, coordinating, capping, and stabilizing agents. Their abundant hydroxyl, carbonyl, and amino functional groups donate electrons to reduce Cu^{2+} and form CuO nuclei, while also coordinating with copper ions to generate transient Cu–ligand complexes that regulate nucleation intensity. During particle growth, these phytochemicals adsorb onto the nanoparticle surfaces through hydrogen bonding, van der Waals interactions, and metal-ligand coordination, forming an organic passivation layer that suppresses uncontrolled crystallite fusion and aggregation. This capping layer provides both steric and electrostatic stabilization, resulting in a controlled size of CuO nanoparticles [33, 34].

The XRD pattern of the synthesized CuO NPs is shown in Fig 3. The observed diffraction peaks at 32.4°, 35.5°, 38.7°, 48.8°, 53.5°, 58.3°, 61.6°, 66.2°, 68.02°, 72.4°, and 75.1°, which correspond to the (002), (-111), (111), (-202), (112), (020), (202), (-113), (022), (-311) and (113) planes of monoclinic CuO (JCPDS 89-2529), respectively [35, 36]. The formation of CuO can be indicated by the presence of diffraction peaks between $2\theta = 35$–$39°$. The average crystallite size of the synthesized CuO NPs can be calculated using the Debye-Scherrer formula as illustrated in Eq. (1):

$$D = \frac{k\lambda}{\beta \cos\theta} \tag{1}$$

where D represents the average crystallite size in nanometers (nm), λ is the X-ray wavelength (0.15406 nm), β is the full width at half maximum (in radian), and θ is the Bragg angle (in degree). After converting the FWHM values from degrees to radians and excluding reflections with extremely narrow FWHM dominated by instrumental broadening, the average crystallite size of the CuO NPs was found to be approximately 82.02 nm. This value is consistent with the particle size observed in the FESEM images.

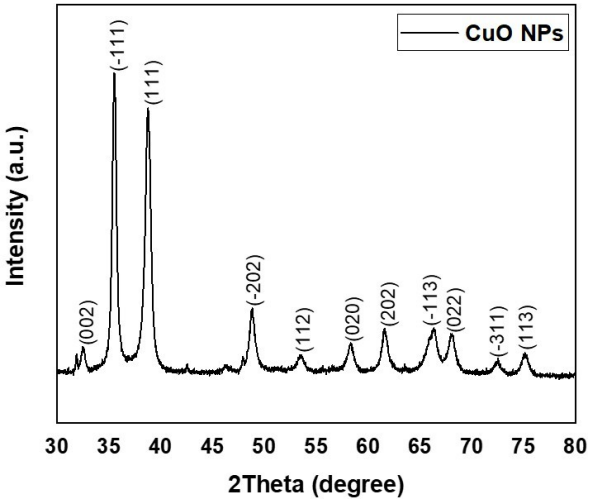

Figure 3: XRD pattern of synthesized CuO NPs

Debye-Scherrer exclusively addresses the influence of crystallite size on peak broadening in XRD diffractions. This analysis fails to account microstructure strains in nanocrystals, including grain boundaries, stacking faults, triple junctions, and point defects. The Williamson-Hall (W–H) plot is commonly used to estimate crystallite size and microstrain of materials. This method represents the microstructural property when microstrain and crystallite combined affect the reflection broadening in the XRD pattern. The size-dependent part relies on the $1/\cos(\theta)$, and the strain-induced part depends on the $\tan(\theta)$. The presence of both small crystallite size and microstrain results in a differentiation of reflection broadening as a function of $\tan\theta$ dependence. The Stokes and Wilson formula is expressed by Eq. (2), representing the strain within the crystals:

$$\beta_{strain} = 4\varepsilon \tan\theta \tag{2}$$

The total broadening of the X-ray diffraction peak (β_{hkl}) is a result of both size broadening (β_{size}) and strain broadening (β_{strain}), which are additive components, as expressed in the following Eq. (3):

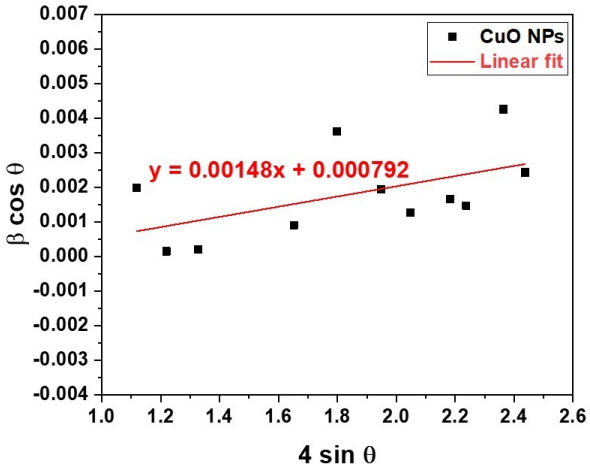

Figure 4: Williamson-Hall (W–H) plot of synthesized CuO NPs

$$\beta_{hkl} = \beta_{size} + \beta_{strain} \tag{3}$$

From the Scherrer and Stokes formula, Eq. (3) can be written as:

$$\beta_{hkl} = \frac{k\lambda}{D\cos\theta} + 4\varepsilon\tan\theta \tag{4}$$

Rearranging Eq. (4) gives:

$$\beta_{hkl}\cos\theta = \frac{k\lambda}{D} + 4\varepsilon\sin\theta \tag{5}$$

The W-H equations (Eq. 5) are represented graphically with $4\sin\theta$ on the x-axis and $\beta_{hkl}\cos\theta$ on the y-axis (Fig. 4). Crystallite size is obtained from the y-intercept, while lattice strain (ε) is calculated from the slope of the linear fit.

The investigation reveals that the average crystallite size is 97.85 nm, while the lattice strain within the synthesized CuO NPs is determined to be 0.792×10^{-3}. The crystallite sizes obtained from the Scherrer and W–H methods are comparable, supporting the reliability of the microstructural parameters. The presence of a small but non-negligible lattice strain indicates that structural imperfections and defects are present in the CuO lattice, as expected for nanoparticles synthesized under relatively mild conditions.

The synthesized CuO NPs revealed antimicrobial efficacy against *E. coli* ATCC 25922 and *S. aureus* ATCC 25923. The MIC values of the synthesized CuO NPs against *E. coli* and *S. aureus* were determined to be 3.98×10^4 and 10.00×10^4 μg/mL, indicating that high concentrations of the synthesized CuO NPs are required to inhibit bacterial growth. The study revealed that MBC for *E. coli* and *S. aureus* was 10×10^4 μg/mL. These results indicated that the bactericidal concentration was also relatively high, with *E. coli* being slightly more susceptible to the synthesized CuO NPs than *S. aureus*. This difference in sensitivity could be attributed to the variations in cell wall structure between *S. aureus* and *E. coli* bacteria, with the thicker peptidoglycan layer in *S. aureus* potentially providing greater resistance to the action of the synthesized CuO NPs.

The antibacterial mechanism of the synthesized CuO NPs involves several key processes. The primary mechanism by which the synthesized CuO NPs exert their antibacterial effect is by generating reactive oxygen species (ROS). When the synthesized CuO NPs encounter bacterial cells, they can catalyze the conversion of molecular oxygen in the surrounding environment into various ROS. These ROS are highly reactive and can cause damage to bacterial cell components, including lipids, proteins, and DNA, leading to cell death. It is important to note that the antibacterial mechanisms of the synthesized CuO NPs are a complex interplay of multiple processes, and their effectiveness can depend on factors such as nanoparticle size, morphology, concentration, and the specific bacterial species targeted [37, 38]. Although activity was observed, the MIC values were relatively high, most likely due to the larger particle size compared with ultrasmall CuO NPs. Future work will focus on optimizing synthesis parameters to reduce particle size and enhance activity.

IV Conclusions

This study demonstrates a successful and environmentally benign synthesis of CuO nanoparticles using *M. speciosa* leaf extract, in which phytochemicals act simultaneously as reducing, chelating, capping, and stabilizing agents. The corrected structural and optical analyses confirmed the formation of phase-pure monoclinic CuO with crystallite sizes of approximately 82–98 nm and an optical band gap of 1.57 eV, consistent with the nanoscale properties of CuO. FESEM observations further revealed quasi-spherical nanoparticles (50–80 nm) with surface texturing arising from phytochemical capping. The antibacterial tests revealed significant activity against Gram-positive (*S. aureus*) and Gram-negative (*E. coli*) bacteria. This green synthesis method provides a sustainable and efficient alternative

to conventional methods, thereby contributing to the development of environmentally responsible nanotechnology. Future work should focus on optimizing synthesis conditions to further reduce particle size, improving antibacterial performance, investigating long-term colloidal stability, and evaluating broader applications in photocatalysis, sensing, and biomedical systems. The insights gained here establish *M. speciosa* as a promising plant-based platform to produce green nanomaterials and encourage its integration into next-generation, eco-friendly nanotechnology frameworks.

Acknowledgments

This research was supported by The Science, Research and Innovation Promotion Funding (TSRI) (Grant no. FRB660012/0168). This research block grant was managed under Rajamangala University of Technology Thanyaburi (FRB66E0627).

[1] R. A. Bapat, C. P. Joshi, P. Bapat, et al., *The use of nanoparticles as biomaterials in dentistry*, Drug Discovery Today, **24**, 85 (2019).

[2] M. Bin Mobarak, M. S. Hossain, F. Chowdhury, and S. Ahmed, *Synthesis and characterization of CuO nanoparticles utilizing waste fish scale and exploitation of XRD peak profile analysis for approximating the structural parameters*, Arabian Journal of Chemistry, **15**, 10 (2022).

[3] L. Rebecchi, N. Petrini, I. Maqueira Albo, N. Curreli, and A. Rubino, *Transparent conducting metal oxides nanoparticles for solution-processed thin films optoelectronics*, Optical Materials: X, **19** (2023).

[4] P. B. Chouke et al., *Bioinspired metal/metal oxide nanoparticles: A road map to potential applications*, Mater Today Adv, **16** (2022).

[5] H. R. Naika et al., *Green synthesis of CuO nanoparticles using Gloriosa superba L. extract and their antibacterial activity*, Journal of Taibah University for Science, **9**, 1 (2015).

[6] P. C. Nagajyothi, P. Muthuraman, T. V. M. Sreekanth, D. H. Kim, and J. Shim, *Green synthesis: In-vitro anticancer activity of copper oxide nanoparticles against human cervical carcinoma cells*, Arabian Journal of Chemistry, **10**, 2 (2017).

[7] Z. Alhalili, *Green synthesis of copper oxide nanoparticles CuO NPs from Eucalyptus Globoulus leaf extract: Adsorption and design of experiments*, Arabian Journal of Chemistry, **15**, 5 (2022).

[8] N. I. I. Zamri, S. L. N. Zulmajdi, E. Kusrini, K. Ayuningtyas, H. M. Yasin, and A. Usman, *Rhodamine b photocatalytic degradation using cuo particles under uv light irradiation for applications in industrial and medical fields*, Evergreen, **7**, 2 (2020).

[9] P. Sable, N. Thabet, J. Yaseen, and G. Dharne, *Effects on Structural Morphological and Optical Properties Pure and CuO/ZnO Nanocomposite*, Trends in Sciences, **19**, 24 (2022).

[10] O. A. Alhamd, G. G. Ali, and M. S. H. Aljuboori, *Study and Characterization of Copper and Titanium Oxides Nanostructures for Some Molecular and Biological Applications*, Trends in Sciences, **21**, 4 (2024).

[11] Y. Wang, D. Wang, B. Yan, Y. Chen, and C. Song, *Fabrication of diverse CuO nanostructures via hydrothermal method and their photocatalytic properties*, Journal of Materials Science: Materials in Electronics, **27**, 7 (2016).

[12] S. Sonia, N. D. Jayram, P. Suresh Kumar, D. Mangalaraj, N. Ponpandian, and C. Viswanathan, *Effect of NaOH concentration on structural, surface and antibacterial activity of CuO nanorods synthesized by direct sonochemical method*, Superlattices Microstruct, **66** (2014).

[13] M. Vila, C. Díaz-Guerra, and J. Piqueras, *Optical and magnetic properties of CuO nanowires grown by thermal oxidation*, J Phys D Appl Phys, **43**, 13 (2010).

[14] A. Benhammada, D. Trache, S. Chelouche, and A. Mezroua, *Catalytic Effect of Green CuO Nanoparticles on the Thermal Decomposition Kinetics of Ammonium Perchlorate*, Z Anorg Allg Chem, **647**, 4 (2021).

[15] K. Phiwdang, S. Suphankij, W. Mekprasart, and W. Pecharapa, *Synthesis of CuO nanoparticles by precipitation method using different precursors*, Energy Procedia, **34** (2013).

[16] H. Suryanto, U. Yanuhar, A. A. Fikri, and G. Mahasri, *Chlorella vulgaris-Mediated Nanosilver Synthesis with Chitosan Capping Agent*, Evergreen, **10**, 1 (2023).

[17] A. S. Rini, Y. Rati, R. Fadillah, R. Farma, L. Umar, and Y. Soerbakti, *Improved Photocatalytic Activity of ZnO Film Prepared via Green Synthesis Method Using Red Watermelon Rind Extract*, Evergreen, **9**, 4 (2022).

[18] M. A. Serunting, O. F. T. Maryana, E. Syafitri, S. Balqis, and E. Windiastuti, *Green synthesis silver nanoparticles (Agnps) using lamtoro pods extract (leucaena leucocephala) and their potential for mercury ion detection*, Evergreen, **8**, 1 (2021).

[19] P. Mohammed Yusuf Ansari, R. M. Muthukrishnan, R. Imran Khan, C. Vedhi, K. Sakthipandi, and S. M. Abdul Kader, *Green synthesis of copper oxide nanoparticles using Amaranthus dubius leaf extract for sensor and photocatalytic applications*, Chemical Physics Impact, **7** (2023).

[20] G. M. Nair, T. Sajini, and B. Mathew, *Advanced green approaches for metal and metal oxide nanoparticles synthesis and their environmental applications*, 2022.

[21] K. Barman, P. Dutta, D. Chowdhury, and P. K. Baruah, *Green Biosynthesis of Copper Oxide Nanoparticles Using Waste Colocasia esculenta Leaves Extract and Their Application as Recyclable Catalyst Towards the Synthesis of 1,2,3-triazoles*, Bionanoscience, **11**, 1 (2021).

[22] B. Bai et al., *Biosynthesized copper oxide nanoparticles (CuO NPs) enhances the antibiofilm efficacy against K. pneumoniae and S. aureus*, J King Saud Univ Sci, **34**, 6 (2022).

[23] D. R. A. Preethi and A. Philominal, *Green Synthesis of Pure and Silver Doped Copper Oxide Nanoparticles using Moringa Oleifera Leaf Extract*, Materials Letters: X, **13** (2022).

[24] S. Logambal et al., *Synthesis and characterizations of CuO nanoparticles using Couroupita guianensis extract for and antimicrobial applications*, J King Saud Univ Sci, **34**, 3 (2022).

[25] A. Atri, M. Echabaane, A. Bouzidi, I. Harabi, B. M. Soucase, and R. Ben Chaâbane, *Green synthesis of copper oxide nanoparticles using Ephedra Alata plant extract and a study of their antifungal, antibacterial activity and photocatalytic performance under sunlight*, Heliyon, **9**, 2 (2023).

[26] E. C. Okpara, O. E. Ogunjinmi, O. A. Oyewo, O. E. Fayemi, and D. C. Onwudiwe, *Green synthesis of copper oxide nanoparticles using extracts of Solanum macrocarpon fruit and their redox responses on SPAu electrode*, Heliyon, **7**, 12 (2021).

[27] F. Gogineni, F. Leon, B. Avery, C. McCurdy, and S. Cutler, *Phytochemistry of Mitragyna speciosa*, Chapter 6 In: Kratom and Other Mitragynines. R.B. Raffa Ed., CRC press, Boca Raton (2014).

[28] R. Yuniarti, S. Nadia, A. Alamanda, M. Zubir, R. A. Syahputra, and M. Nizam, *Characterization, Phytochemical Screenings and Antioxidant Activity Test of Kratom Leaf Ethanol Extract (Mitragyna speciosa Korth) Using DPPH Method*, Journal of Physics: Conference Series (2020).

[29] F. Zakaria, J. K. Tan, S. M. Mohd Faudzi, M. B. Abdul Rahman, and S. E. Ashari, *Ultrasound-assisted extraction conditions optimisation using response surface methodology from Mitragyna speciosa (Korth.) Havil leaves*, Ultrason Sonochem, **81** (2021).

[30] G. H. Al-Hazmi, M. G. El-Desouky, and A. A. El-Bindary, *SYNTHESIS, CHARACTERIZATION AND MICROSTRUCTURAL EVALUATION OF ZnO NANOPARTICLES BY WILLIAM-HALL AND SIZE-STRAIN PLOT METHODS*, Bull Chem Soc Ethiop, **36**, 4 (2022).

[31] K. Patel, A. Patel, V. P. Jethwa, H. Patel, and G. K. Solanki, *X-ray diffraction analysis of orthorhombic SnSe nanoparticles by Williamson–Hall, Halder–Wagner and Size–Strain plot methods*, Chemical Physics Impact, **8** (2024).

[32] M. M. Ilmi, N. Nurdini, E. Maryanti, P. Setiawan, and I. Ismunandar, *X-ray Diffraction Peak Profile for Determination of Microstructural Properties of Hematite (Fe2O3)*, Journal of Research and Development on Nanotechnology, **1**, 1 (2021).

[33] S. Iravani, *Green synthesis of metal nanoparticles using plants*, Green Chemistry, **13**, 10 (2011).

[34] N. Anwar, M. Shah, S. Saleem, and H. Rahman, *Plant mediated synthesis of silver nanoparticles and their biological applications*, Bull Chem Soc Ethiop, **32**, 3 (2018).

[35] E. Abbasi, M. Haghighi, R. Shokrani, and M. Shabani, *Copper plasmon-induced Cu-doped ZnO-CuO double-nanoheterojunction: In-situ combustion synthesis and photo-decontamination of textile effluents*, Mater Res Bull, **129** (2020).

[36] R. Rajamohan, C. J. Raorane, S. C. Kim, and Y. R. Lee, *One Pot Synthesis of Copper Oxide Nanoparticles for Efficient Antibacterial Activity*, Materials, **16**, 1 (2023).

[37] G. Applerot et al., *Understanding the antibacterial mechanism of CuO nanoparticles: Revealing the route of induced oxidative stress*, Small, **8**, 21 (2012).

[38] S. Meghana, P. Kabra, S. Chakraborty, and N. Padmavathy, *Understanding the pathway of antibacterial activity of copper oxide nanoparticles*, RSC Adv, **5**, 16 (2015).